Article

Discovery Medicine 2025; 37(202): 2673–2686
https://doi.org/10.24976/Discov.Med.202537202.224

TMAVA Exacerbates Coronary Heart Disease via BBOX-Mediated Mitochondrial Dysfunction

Zhen Ma[1], Dong Wu[2], Wenguang Liu[1], Yingjie Guo[1], Bin Ning[1,*]

[1]Department of Cardiovascular Medicine, Fuyang Hospital of Anhui Medical University (Fuyang People's Hospital), 230022 Fuyang, Anhui, China
[2]Department of Pharmacy, Fuyang Hospital of Anhui Medical University (Fuyang People's Hospital), 230022 Fuyang, Anhui, China
*Correspondence: 117525538@qq.com (Bin Ning)

Submitted: 15 August 2025 Revised: 12 September 2025 Accepted: 24 September 2025 Published: 20 November 2025

Background: N,N,N-trimethyl-5-aminovaleric acid (TMAVA), a lysine-derived metabolite generated by gut microbiota, has been associated with metabolic disorders. However, its role in cardiovascular disease remains unclear. This study aimed to investigate whether TMAVA promotes atherosclerosis progression by disrupting mitochondrial metabolism through inhibition of γ-butyrobetaine hydroxylase (BBOX), a key enzyme in carnitine biosynthesis.

Methods: *In vivo*, ApoE$^{-/-}$ mice were fed a high-fat diet and treated with TMAVA, with or without concurrent BBOX overexpression, for eight weeks. *In vitro*, human umbilical vein endothelial cells (HUVECs) were exposed to TMAVA, with or without *BBOX* overexpression, or left untreated. Molecular, metabolic, and functional assays were conducted to evaluate lipid metabolism, mitochondrial function, inflammation, and endothelial function.

Results: TMAVA accumulated in the aortic tissue of ApoE$^{-/-}$ mice ($p < 0.05$) and was associated with aggravated lipid profiles ($p < 0.05$), increased inflammatory cytokine expression ($p < 0.05$), and impaired mitochondrial function ($p < 0.05$). In HUVECs, TMAVA further exacerbated ox-LDL-induced mitochondrial damage, oxidative stress, and inflammation ($p < 0.05$), accompanied by significant reductions in carnitine levels, ATP production, and fatty acid oxidation markers (AMPK, CPT1α) ($p < 0.05$). *BBOX* overexpression restored mitochondrial function and reversed TMAVA-induced metabolic and inflammatory abnormalities in both models ($p < 0.05$).

Conclusion: TMAVA accelerates atherosclerosis by suppressing BBOX expression, impairing carnitine biosynthesis, and disrupting mitochondrial fatty acid oxidation, ultimately leading to endothelial dysfunction and vascular inflammation. Targeting the TMAVA-BBOX-carnitine pathway may represent a promising therapeutic strategy for cardiovascular disease.

Keywords: TMAVA; BBOX; carnitine; fatty acid oxidation; mitochondrial dysfunction; endothelial inflammation; atherosclerosis

Introduction

Coronary heart disease (CHD), responsible for 17.9 million deaths annually (32% of global mortality according to the World Health Organization), remains a leading global health burden [1,2]. In China, the prevalence of CHD has risen significantly in recent years, now affecting more than 11 million individuals and imposing a considerable healthcare burden [3,4]. Despite advances in pharmacological therapies and interventional procedures, residual cardiovascular risk persists, particularly among individuals with underlying metabolic disorders.

Accumulating evidence indicates that metabolic dysregulation, especially impaired mitochondrial energy metabolism, is a central mechanism driving atherosclerosis progression [5–7]. Because mitochondria are the primary source of energy in vascular and cardiac cells, dysfunction in fatty acid oxidation (FAO) can result in energy imbalance, oxidative stress, and sustained endothelial inflammation [8,9], all of which accelerate atherogenesis. Recent findings highlight the gut microbiota as a critical regulator of host metabolism and cardiovascular health [10]. However, the molecular mechanisms by which microbial metabolites impair mitochondrial function and promote CHD progression remain poorly defined.

N,N,N-trimethyl-5-aminovaleric acid (TMAVA) is a gut microbiota-derived metabolite generated from lysine degradation by taxa such as *Enterococcus* and *Lactobacillus* [11,12]. It functions as a potent endogenous inhibitor of γ-butyrobetaine hydroxylase (BBOX), the key enzyme in carnitine biosynthesis [13,14]. Carnitine is essential for mitochondrial β-oxidation of long-chain fatty acids, the principal energy-generating pathway in endothelial and myocardial cells [15]. TMAVA-mediated inhibition of BBOX reduces carnitine availability, impairs fatty acid transport, and compromises mitochondrial oxidative phosphorylation. Previous research has shown that TMAVA accumulation contributes to metabolic disorders, including obesity, fatty liver disease, and insulin resistance [16]. Moreover, TMAVA has been associated with elevated mitochondrial reactive oxygen species (ROS), impaired ATP generation, and loss of mitochondrial membrane potential [17]. Despite

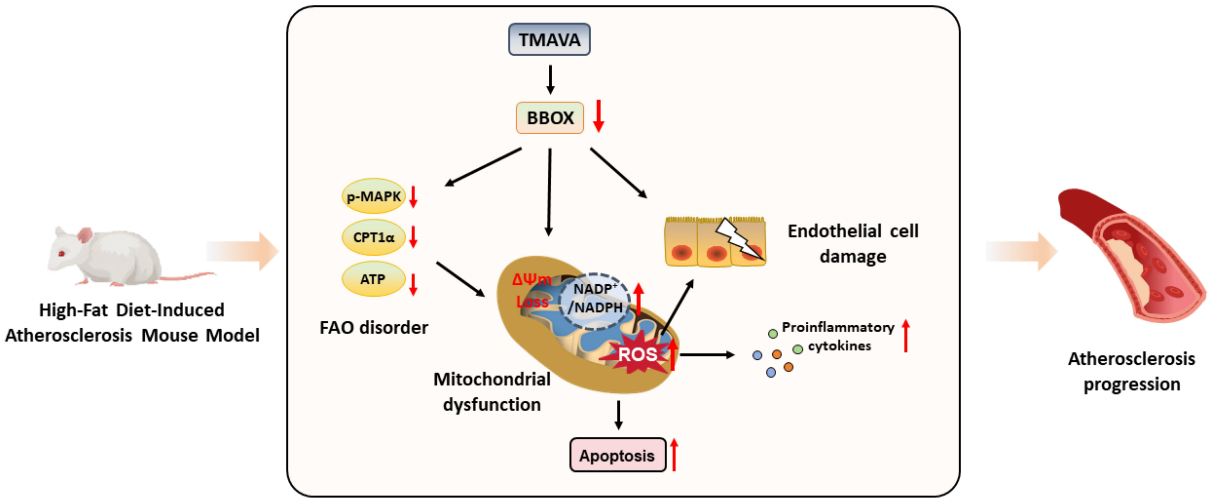

Fig. 1. Proposed mechanism by which TMAVA accelerates atherosclerosis via BBOX-mediated mitochondrial dysfunction. The schematic illustration was created using Adobe Illustrator (Adobe Inc., San Jose, CA, USA). Red arrows indicate the direction of expression or activity changes: upward arrows (↑) represent upregulation or increase, while downward arrows (↓) represent downregulation or decrease. TMAVA, N,N,N-trimethyl-5-aminovaleric acid; BBOX, γ-butyrobetaine hydroxylase; P-MAPK, phosphorylated mitogen-activated protein kinase; CPT1α, carnitine palmitoyltransferase 1 alpha; ATP, adenosine triphosphate; ROS, reactive oxygen species; FAO, fatty acid oxidation.

these findings, the contribution of TMAVA to cardiovascular disease, especially endothelial injury and atherosclerosis, has not been systematically investigated. It also remains unknown whether restoring BBOX expression can rescue TMAVA-induced mitochondrial dysfunction in vascular systems. Thus, the role of TMAVA in CHD and its regulation of mitochondrial metabolism through BBOX inhibition represent a significant gap in current knowledge. Furthermore, the therapeutic potential of targeting the TMAVA-BBOX axis in atherosclerosis has not been determined.

This study aimed to determine whether TMAVA exacerbates CHD by inhibiting BBOX and inducing mitochondrial dysfunction. We evaluated the *in vivo* effects of TMAVA and *BBOX* overexpression in ApoE^{-}/$^{-}$ mice, focusing on lipid metabolism and vascular inflammation. *In vitro*, we examined mitochondrial function, oxidative stress, apoptosis, and cell viability in human umbilical vein endothelial cells (HUVECs) exposed to TMAVA, with or without *BBOX* rescue. This integrated approach provides mechanistic insight into the pathogenic role of the TMAVA-BBOX-mitochondrial axis in CHD. A schematic diagram illustrating the proposed TMAVA-BBOX-carnitine-mitochondrial pathway underlying atherosclerosis progression is presented in Fig. 1.

Materials and Methods

Experimental Design and Treatments

To investigate the role of TMAVA and BBOX in CHD and mitochondrial dysfunction, both *in vivo* and *in vitro* models were employed. For the *in vivo* atherosclerosis model, twenty male ApoE^{-}/$^{-}$ mice (6 weeks old) were purchased from Cyagen Biosciences Inc. (Guangzhou, China) and randomly assigned into four groups (n = 5 per group): (1) Control group receiving a standard chow diet and distilled water. The chow diet contained approximately 20% protein, 4–5% fat, 55–60% carbohydrates, plus standard vitamins and minerals; (2) High-fat diet (HFD) group receiving a high-fat diet composed of 10% lard, 2% cholesterol, 0.2% propylthiouracil, and 0.5% sodium cholate; (3) HFD + TMAVA group receiving 0.325% TMAVA (w/v) in drinking water; and (4) HFD + TMAVA + *BBOX* group receiving TMAVA and intraperitoneal injection of *BBOX*-overexpressing lentivirus (titer: 1×10^{8} TU/mL, 100 µL per injection).

All interventions were administered for 8 weeks [18]. Serum, aortic, and liver samples were collected for biochemical and molecular analyses. Before sample collection, mice were humanely euthanized via intraperitoneal injection of pentobarbital sodium (≥150 mg/kg body weight),

with death confirmed by cessation of respiration and heartbeat, in accordance with institutional animal care guidelines. All animal procedures complied with NIH Guidelines and were approved by the Institutional Animal Care and Use Committee of the Guangdong Provincial Center for Laboratory Animals (No. D202506-13).

In vitro, HUVECs were obtained from Procell Life Science & Technology Co., Ltd. (Wuhan, China) and cultured in ECM medium supplemented with 10% FBS and 1% penicillin-streptomycin at 37 °C under 5% CO_2. The supplier provided short tandem repeat (STR) profiling for authentication, and cell line identity was verified. Routine mycoplasma testing was performed using a commercial detection kit (HY-K0552, MedChemExpress, USA), and all results were negative. When culture reached 80–90% confluence, cells were digested with 0.25% trypsin-0.02% ethylenediaminetetraacetic acid (EDTA), neutralized with complete medium, centrifuged, and resuspended for further experiments.

To assess TMAVA toxicity, HUVECs were treated with increasing concentrations of TMAVA (0.5, 1, 2.5, 5, 10, and 20 µmol/L) for 24 h, followed by 3-(4,5-dimethylthiazol-2-yl)-2,5-diphenyltetrazolium bromide (MTT) assay to determine sub-cytotoxic concentrations. To evaluate dose-dependent effects of TMAVA under oxidative stress, HUVECs were divided into five groups: (1) control; (2) positive control (ox-LDL 100 µg/mL for 12 h); and (3–5) ox-LDL + TMAVA groups exposed sequentially to ox-LDL and TMAVA (2.5, 5, or 10 µmol/L for 24 h) [19].

To determine whether *BBOX* overexpression mitigates TMAVA-induced dysfunction, HUVECs were transduced with a recombinant lentiviral vector encoding full-length human *BBOX* (GenBank accession no. NM_001256226) cloned into the pLV-eGFP-N-Puro backbone (Sangon Biotech, Shanghai, China). Detailed vector and coding sequence information is provided in **Supplementary Fig. 1** and **Supplementary Table 1**. HUVECs were seeded in 6-well plates at 2×10^5 cells/well. When cells reached 60–70% confluence, transduction was performed at a multiplicity of infection (MOI) of 20 in the presence of 8 µg/mL polybrene (Sigma-Aldrich, USA). After 24 h, the medium was replaced with fresh complete medium, and cells were cultured for an additional 48 h before subsequent treatments. Transduction efficiency was verified by GFP fluorescence microscopy and validated by BBOX mRNA expression. Transduction was performed 24 h prior to ox-LDL exposure.

Cells were assigned into four groups: (1) control; (2) ox-LDL; (3) ox-LDL + TMAVA (10 µmol/L); and (4) ox-LDL + TMAVA + *BBOX*. After treatment, cells were harvested for assessment of ROS levels, ATP content, carnitine levels, mitochondrial membrane potential, and apoptosis.

High-Performance Liquid Chromatography

TMAVA levels in mouse aortic tissue were quantified using high-performance liquid chromatography (HPLC) (Shimadzu LC-10AT) equipped with a UV detector and a C18 reverse-phase column (250 mm × 4.6 mm, 5 µm). Aortic tissues were homogenized in 1 mL of HPLC-grade methanol (Merck, Germany), sonicated on ice for 10 min, and centrifuged at 12,000 rpm for 10 min at 4 °C. The supernatant was passed through a 0.22 µm syringe filter. The mobile phase consisted of acetonitrile and 0.1% formic acid in water (30:70, v/v) at a flow rate of 1.0 mL/min. Detection was performed at 210 nm, and TMAVA concentrations were calculated using a standard calibration curve ($R^2 > 0.99$).

Enzyme-Linked Immunosorbent Assay

Serum levels of high-density lipoprotein cholesterol (HDL-C), total cholesterol (TC), serum triglycerides (TG), and low-density lipoprotein cholesterol (LDL-C) were measured using commercial ELISA kits (ml095894, ml037202, ml037765, ml037825; Enzyme-linked Biotechnology, China). Intracellular ATP and total carnitine in HUVECs were quantified using ATP ELISA kits (YS02421B, Yaji Biotech, China) and carnitine kits (JN6889, Jining Biotech, China). Absorbance was measured at 450 nm, and values were normalized to total protein concentration. All assays were performed in triplicate using standard curves for quantification.

Quantitative Reverse Transcription PCR

Total RNA was extracted from mouse aortic tissues or HUVECs using the Cell/Tissue Total RNA Isolation Kit V2 (Vazyme, China), and reverse-transcribed into cDNA with the HiScript III 1stStrand cDNA Synthesis Kit (Vazyme, China). RT-qPCR was performed with SYBR qPCR Master Mix (Vazyme, China) on a CFX96 Touch Real-Time PCR System (Bio-Rad). To validate BBOX overexpression (Fig. 6B), total RNA was extracted from transduced HUVECs and analyzed. Primer sequences for mouse genes are listed in Table 1, and those for human BBOX are provided in Table 2. *GAPDH* was used as the internal reference, and relative expression levels were calculated using the $2^{-\Delta\Delta Ct}$ method. All primers were synthesized by Sangon Biotech (Shanghai, China).

Western Blotting

Protein was extracted from aortic tissue and HUVECs using RIPA lysis buffer (Beyotime, China) supplemented with 1 mM PMSF and quantified using a BCA assay kit (NCM Biotech, China). Equal amounts of protein (20–40 µg per sample) were separated by 10% SDS-PAGE and subsequently transferred onto PVDF membranes (0.22 µm; Millipore, Merck, Germany) using a Trans-Blot system (Bio-Rad, USA). Membranes were blocked with

Table 1. Primer sequences of *Mus musculus* used for RT-qPCR analysis in aortic tissues.

Gene	Primer Sequences (5′→3′)
TNF-α	Forward: GAATGTCCATTCCTGAGTTCTG
	Reverse: TTCTCTCAATGACCCGTAGG
IL-6	Forward: AGAAAGACAAAGCCAGAGTCC
	Reverse: AATGTCCACAAACTGATATGCTTAGG
IL-1β	Forward: AAAGATGAAGGGCTGCTTCC
	Reverse: GCTTTCAGCTCATATGGGTC
GAPDH	Forward: TTAGGTTCATCAGGTAAACTCAGG
	Reverse: TTCTCGGCCTTGACTGTGC

TNF-α, tumor necrosis factor-alpha; *IL-6*, interleukin-6; *IL-1β*, interleukin-1 beta; *GAPDH*, glyceraldehyde-3-phosphate dehydrogenase.

Table 2. Primer sequences of *Homo sapiens* used for RT-qPCR in HUVECs.

Gene	Primer Sequences (5′→3′)
TNF-α	Forward: TATCCTGGGGGACCCAATGT
	Reverse: AAAGAAGGCACAGAGGCCAG
IL-6	Forward: TTCTCCACAATACCCCCAGGAG
	Reverse: CTGAGATGCCGTCGAGGATG
IL-1β	Forward: GCCCTAAACAGATGAAGTGC
	Reverse: CCATGTGTCGAAGAAGATAGG
BBOX1	Forward: CAGACATTGGAGTGGATTACTGTG
	Reverse: GGCTGAACTCTTTCAACAGGCAC
GAPDH	Forward: AAGATCATCAGCAATGCCTCC
	Reverse: AGGTTTTTCTAGACGGCAGG

BBOX1, γ-butyrobetaine hydroxylase 1.

5% BSA in TBST for 1 h at room temperature and incubated overnight at 4 °C with the following antibodies: anti-BBOX1 (1:1000, ab171959, Abcam), anti-IL-6 (1:500, ab233706, Abcam), anti-TNF-α (1:2000, ab183218, Abcam), anti-CPT1α (1:1000, ab220789, Abcam), anti-IL-1β (1:1000, ab254360, Abcam), and anti-phospho-AMPK (p-AMPK; 1:1000, ab133448, Abcam). After washing with TBST, membranes were incubated for 1 h at room temperature with horseradish peroxidase (HRP)-conjugated secondary antibodies (Bioss, China): goat anti-rabbit IgG H&L (HRP) (Cat# bs-0295G-HRP; for rabbit primary antibodies) or goat anti-mouse IgG H&L (HRP) (Cat# bs-0296G-HRP; for mouse primary antibodies), both diluted 1:5000. Immunoreactive bands were visualized with enhanced chemiluminescence (ECL) reagents (NCM Biotech, China) and captured using a ChemiDoc imaging system (Bio-Rad, USA). Band intensities were quantified with ImageJ software (version 1.53t, National Institutes of Health, Bethesda, MD, USA) and normalized to GAPDH (mouse monoclonal, Abcam, Cat# ab8245, 1:5000), which served as the internal control.

Detection of Mitochondrial ROS

HUVECs in different treatment groups were seeded into 24-well plates at a density of 1×10^5 cells/well. Upon reaching approximately 80% confluence, cells were washed twice with PBS and incubated with 200 nM Mito-Tracker Red CMXRos (from a 200 μM stock diluted in culture medium) and the green fluorescent probe BBcellProbe® OM09 (excitation/emission = 488/510 nm) at 37 °C for 30 min in the dark. Following three PBS washes, stained cells were imaged within 2 h using a fluorescence microscope.

Detection of Mitochondrial Membrane Potential

Mitochondrial membrane potential (ΔΨm) was assessed by JC-1 staining. A working solution was prepared by diluting 30 μL of JC-1 stock (200×) and 1.2 mL of 5× JC-1 buffer in ultrapure water to a final volume of 6 mL. HUVECs cultured in 6-well plates were treated according to protocol, washed once with PBS, and incubated with 1 mL of JC-1 working solution at 37 °C for 20 min. Cells were subsequently washed twice with 1× JC-1 buffer, resuspended in culture medium, and examined under a fluorescence microscope (Nikon, Japan).

Flow Cytometry

Apoptosis was evaluated using Annexin V-FITC/PI dual staining (Thermo Fisher Scientific, USA). Following treatment, HUVECs (1×10^6 cells/well) were harvested, washed twice with PBS, and resuspended in 100 μL of 1× Annexin V binding buffer. Cells were then stained with 5 μL Annexin V-FITC and 5 μL propidium iodide (PI) under dark conditions at room temperature for 15 min, followed by dilution with 400 μL binding buffer. Samples were analyzed within 1 h using an Attune NxT flow cytometer (Thermo Fisher) with no fewer than 10,000 events collected per experimental sample. Data were processed with FlowJo software (BD Biosciences, USA), and the proportions of early (Annexin V^+/PI^-) and late (Annexin V^+/PI^+) apoptotic cells were quantified.

WST-8 Assay

The intracellular $NADP^+$/NADPH ratio was determined using a colorimetric WST-8 assay kit (Beyotime, China). HUVECs (1×10^6 cells/well) were seeded into 6-well plates and treated according to the experimental protocols. Cell lysates were centrifuged at 12,000 ×g for 10 min at 4 °C. For NADPH-specific measurement, aliquots were pre-heated at 60 °C for 30 min to degrade $NADP^+$. Subsequently, 50 μL supernatant was transferred to 96-well plates, followed by 50 μL of G6PDH working solution and incubation at 37 °C for 10 min. 10 μL WST-8 solution was then added, and plates were incubated for an additional 20–30 min in the dark. Absorbance was measured at 450 nm using a microplate reader (RT-6000, Rayto, China). The $NADP^+$/NADPH ratio was calculated from a standard curve (0–8 μM).

MTT Assay

Cell viability was assessed via seeding HUVECs (1×10^4/well) into 96-well plates. Following treatment, each well was then incubated with 10 µL of MTT solution (0.5 mg/mL) for 4 h at 37 °C. The resulting formazan crystals were solubilized in 100 µL DMSO, and absorbance at 570 nm was determined using a microplate reader (RT-6000, Rayto, China).

CCK-8 Assay

Cell proliferation was evaluated with a CCK-8 assay kit. HUVECs, either untreated or successfully transfected, were seeded into 96-well plates at a density of 2000 cells/well. When cells reached 80% confluence, treatments were applied as per experimental grouping requirements. Two hours before the end of incubation, 10 µL of CCK-8 reagent (final concentration 10%) was added to each well. After incubation, absorbance at 450 nmwas measured using a microplate reader (RT-6000, Rayto, China). Cell proliferation was expressed as: OD_{450} (experimental)/OD_{450} (control) $\times$ 100%.

Transwell Invasion Assay

Cell invasion was evaluated using Matrigel-coated Transwell chambers (8 µm pore size; Corning, China). The upper chambers were seeded with HUVECs (2×10^5/mL) in serum-free medium, whereas the lower chambers were filled with complete medium. Cells were pretreated with ox-LDL (100 µg/mL, 12 h), followed by TMAVA (2.5, 5, or 10 µmol/L, 24 h). Following incubation, non-invading cells were removed, and invaded cells were fixed, stained with crystal violet, and quantified microscopically (Olympus, Japan) in five randomly selected fields.

Scratch Wound Healing Assay

HUVECs were seeded into 6-well plates (1×10^6 cells/well). Upon reaching approximately 80% confluence, a linear wound was introduced using a sterile pipette tip. After two PBS washes, the baseline wound width was recorded by imaging. Cells were then treated according to experimental grouping, and wound closure was evaluated by capturing images at 24 h and 48 h post-scratch.

Statistical Analysis

All statistical analyses were performed using SPSS version 26.0 (IBM Corp., Armonk, NY, USA). Data are expressed as mean $\pm$ standard deviation (SD). Multiple group comparisons were assessed using one-way analysis of variance (ANOVA) followed by Tukey's post hoc test. A p-value < 0.05 was considered statistically significant. Each experiment was performed in independent triplicate.

Results

TMAVA Accumulates in Aortic Tissue of ApoE$^{-/-}$ Mice Fed a High-Fat Diet

To investigate whether dietary and microbial factors influence TMAVA accumulation in vascular tissue, TMAVA levels in the aorta of ApoE$^{-/-}$ mice were measured by HPLC. Chromatographic profiles revealed a markedly elevated TMAVA peak in the HFD group compared with the control group. Quantitative analysis confirmed that TMAVA content was significantly higher in the HFD group compared with the control group ($p < 0.05$) (Fig. 2A). Moreover, TMAVA levels were modestly but significantly elevated in the HFD + TMAVA group compared with the HFD group ($p < 0.05$) (Fig. 2B), indicating that both high-fat feeding and exogenous TMAVA contribute to aortic TMAVA accumulation.

TMAVA Exacerbates Lipid Metabolism Disorder and Inflammatory Response in ApoE$^{-/-}$ Mice

To evaluate the effects of TMAVA on lipid homeostasis *in vivo*, serum lipid profiles were assessed in ApoE$^{-/-}$ mice. As shown in Fig. 3A, HFD feeding significantly increased serum TG, TC, and LDL-C levels while decreasing HDL-C compared with controls ($p < 0.05$). TMAVA administration further aggravated these changes, suggesting exacerbation of HFD-induced dyslipidemia. Vascular inflammation was assessed by examining inflammatory cytokine expression in aortic tissue. RT-qPCR analysis revealed increased mRNA expression of *IL-6*, *TNF-*α, and *IL-1*β in the HFD group, which was further elevated by TMAVA treatment (Fig. 3B; $p < 0.05$). Consistently, Western blot results confirmed higher protein levels of these cytokines, with the HFD + TMAVA group exhibiting the greatest expression (Fig. 3C; $p < 0.05$). These findings demonstrate that TMAVA amplifies lipid dysregulation and vascular inflammation under high-fat dietary conditions.

TMAVA Aggravates ox-LDL-Induced Endothelial Dysfunction and Inflammation in HUVECs

To determine the functional impact of TMAVA on endothelial cells under oxidative stress, HUVECs were exposed to ox-LDL with or without escalating concentrations of TMAVA. MTT assays confirmed that TMAVA up to 10 µmol/L had no cytotoxic effect within 48 h, while 20 µmol/L significantly reduced viability (Fig. 4A; $p < 0.05$). Thus, concentrations of 2.5, 5, and 10 µmol/L were selected for subsequent experiments. CCK-8 assays (Fig. 4B) demonstrated that ox-LDL markedly suppressed cell proliferation, which was further suppressed by TMAVA in a dose-dependent manner ($p < 0.05$). Wound healing (Fig. 4C; $p < 0.05$) and Transwell invasion assays (Fig. 4D; $p < 0.05$) demonstrated that TMAVA exacerbated ox-LDL-induced impairments in cell migration and invasion, with the high-dose group exhibiting the most pronounced in-

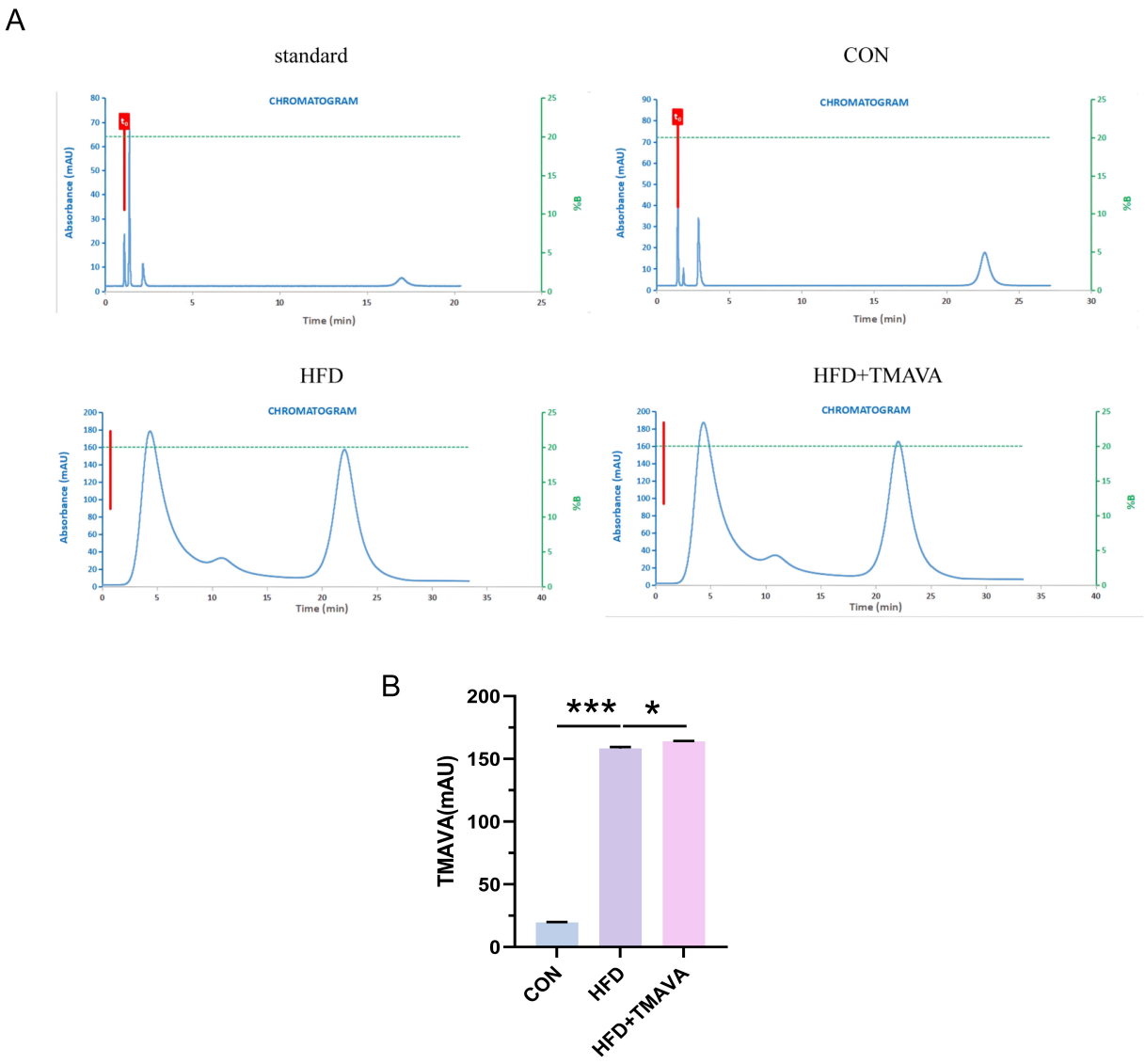

Fig. 2. HPLC analysis of TMAVA levels in aortic tissues of ApoE$^{-/-}$ mice following HFD feeding and exogenous TMAVA administration. (A) Representative HPLC chromatograms showing TMAVA peaks in standard solution and aortic tissues from each group. (B) Quantitative analysis of TMAVA concentration expressed as milli-absorbance units (mAU). *$p < 0.05$, ***$p < 0.001$. HPLC, high-performance liquid chromatography; HFD, high-fat diet.

hibition. Flow cytometry analysis (Fig. 4E) revealed increased apoptosis rates in the positive control group (ox-LDL 100 µg/mL for 12 h), which were further amplified by TMAVA treatment, especially at 10 µmol/L (ox-LDL + L-TMAVA group) ($p < 0.05$). Consistently, ELISA (Fig. 4F) confirmed that TMAVA further enhanced ox-LDL-induced secretion of IL-6, TNF-α, and IL-1β in a concentration-dependent manner ($p < 0.05$).

These findings suggest that TMAVA aggravates ox-LDL-induced endothelial dysfunction by suppressing proliferation and migration, promoting apoptosis, and enhancing inflammatory cytokine production.

TMAVA Aggravates Mitochondrial Dysfunction and Impairs Fatty Acid Oxidation in ox-LDL-Stimulated HUVECs

To determine whether TMAVA aggravates mitochondrial injury induced by ox-LDL, mitochondrial ROS levels were examined using Mito-Tracker Red CMXRos staining (Fig. 5A). Ox-LDL markedly elevated mitochondrial ROS compared with controls ($p < 0.05$), and TMAVA further enhanced accumulation in a dose-dependent manner. JC-1 demonstrated a markedly reduced red/green fluorescence ratio in the ox-LDL group (Fig. 5B; $p < 0.05$), indicating mitochondrial depolarization, which was further worsened by TMAVA treatment at all concentrations.

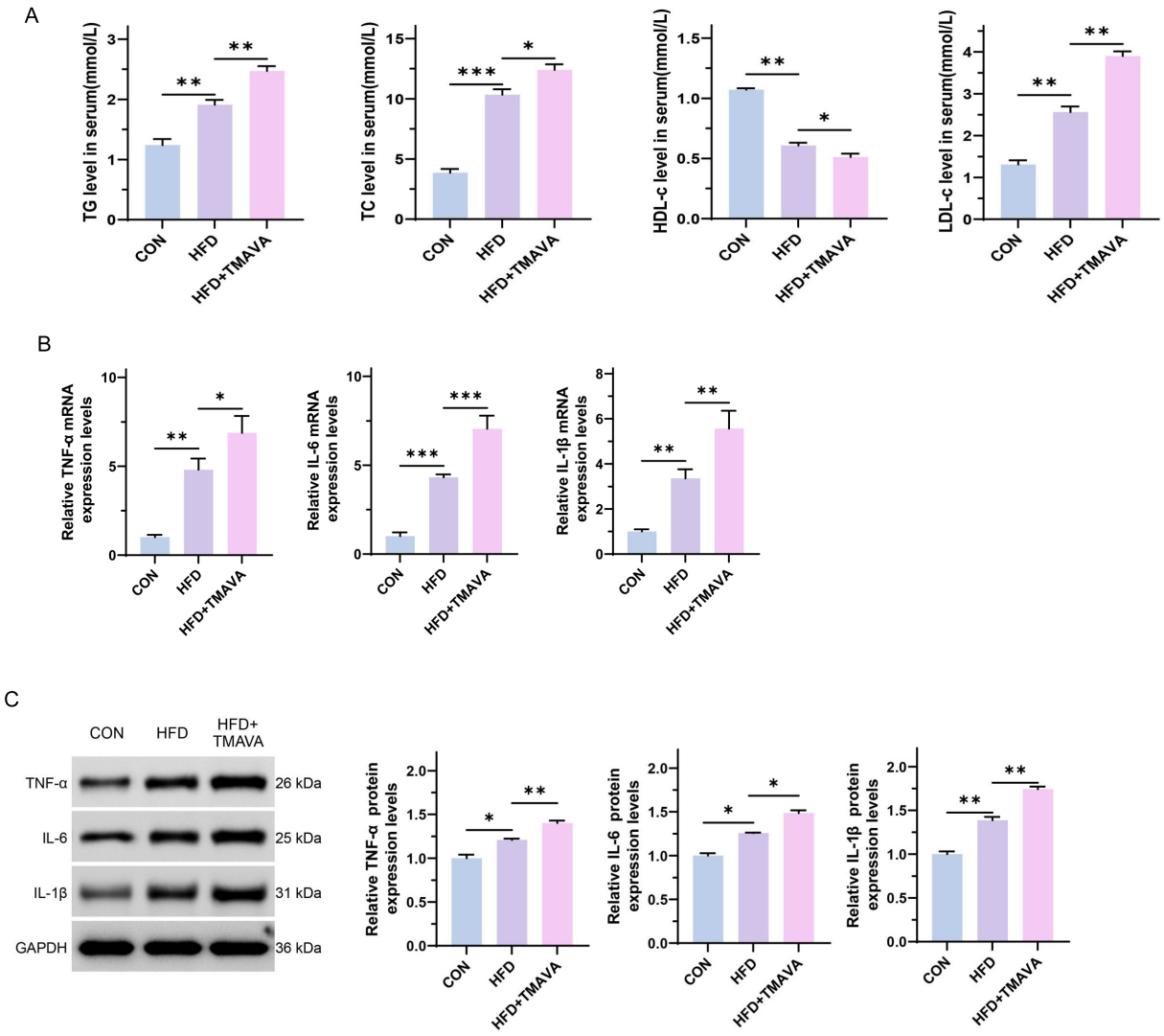

Fig. 3. TMAVA aggravates lipid dysregulation and vascular inflammation in ApoE$^{-/-}$ mice. (A) Serum levels of TG, TC, HDL-C, and LDL-C measured by ELISA across treatment groups. (B) Relative mRNA expression of *TNF-α*, *IL-6*, and *IL-1β* in aortic tissues assessed by RT-qPCR. (C) Western blot and quantitative analyses of TNF-α, IL-6, and IL-1β protein levels in aortic tissues, with GAPDH as the loading control. Data are expressed as mean ± SD. *$p < 0.05$, **$p < 0.01$, ***$p < 0.001$. TG, serum triglycerides; TC, total cholesterol; HDL-C, high-density lipoprotein cholesterol; LDL-C, low-density lipoprotein cholesterol; ELISA, enzyme-linked immunosorbent assay.

To evaluate mitochondrial metabolic capacity, intracellular carnitine and ATP levels were quantified by ELISA (Fig. 5C,D). Both parameters were significantly reduced by ox-LDL ($p < 0.05$), with TMAVA inducing further concentration-dependent decreases. Redox imbalance was assessed using the $NADP^+$/NADPH ratio (WST-8 assay, Fig. 5E). TMAVA markedly increased the ratio beyond that induced by ox-LDL alone ($p < 0.05$), suggesting exacerbated oxidative stress. Western blot analysis revealed that ox-LDL suppressed p-AMPK and CPT1α expression, key regulators of mitochondrial energy metabolism and fatty acid oxidation, and TMAVA treatment further downregulated both proteins, particularly at medium and high concentrations (Fig. 5F).

These findings indicate that TMAVA worsens mitochondrial dysfunction and inhibits fatty acid oxidation by promoting ROS accumulation, membrane depolarization, redox imbalance, and impaired metabolic signaling in ox-LDL-stimulated endothelial cells.

BBOX Overexpression Restores Carnitine Metabolism and Mitochondrial Function in TMAVA-Treated HUVECs

To assess whether *BBOX* overexpression mitigates TMAVA-induced mitochondrial dysfunction, we first examined the expression of BBOX. Fig. 6A shows that TMAVA significantly reduced BBOX protein levels in ox-LDL-treated HUVECs, especially at high concentrations (*p*

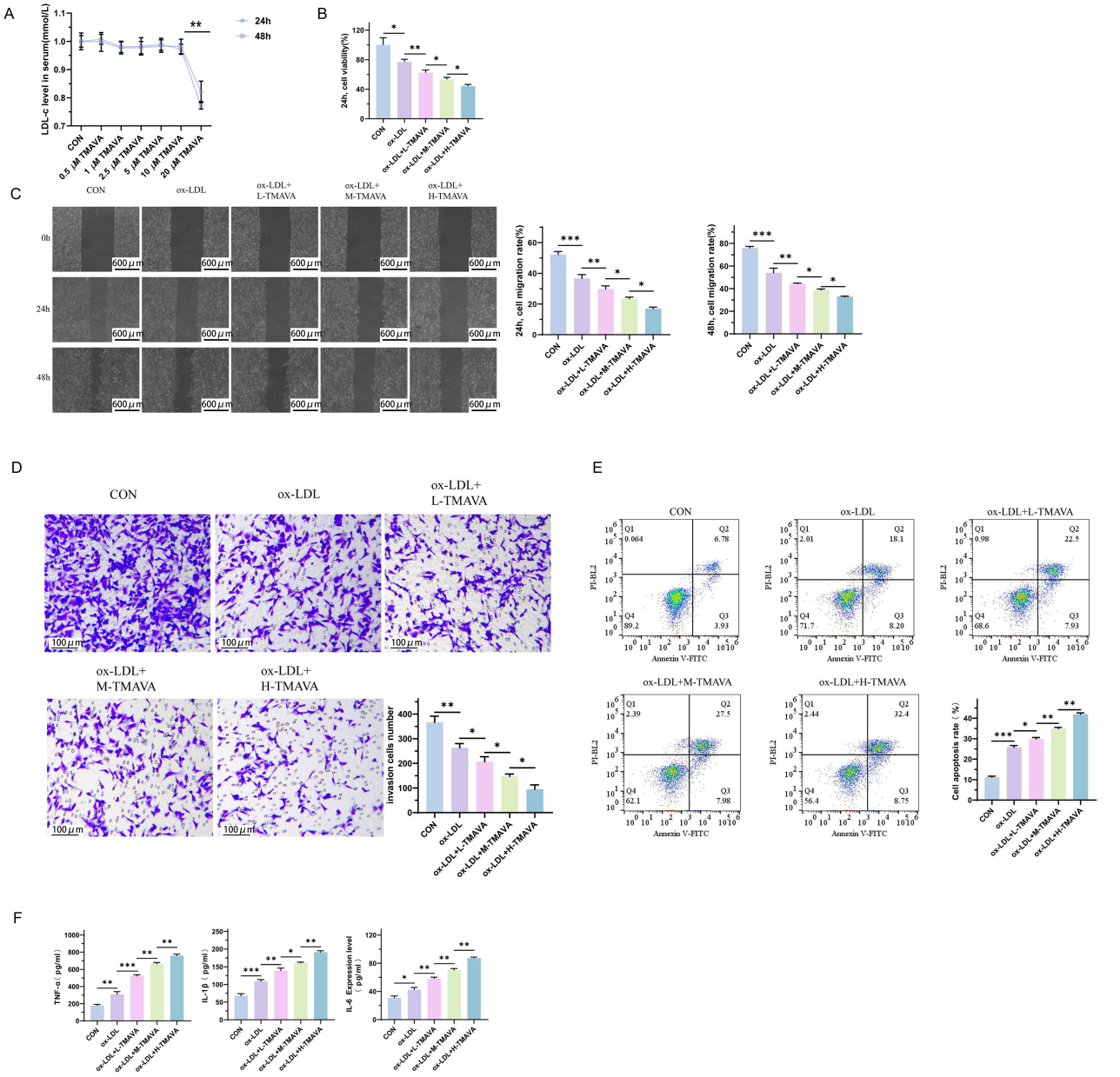

Fig. 4. TMAVA aggravates ox-LDL-induced endothelial dysfunction and inflammation in HUVECs. (A) Cell viability determined by MTT assay following 24 and 48 h of treatment. (B) Cell proliferation assessed using the CCK-8 assay in each group. (C) Cell migration evaluated by wound healing assay at 0, 24, and 48 h in each group. (D) Invasive capacity of HUVECs under each treatment analyzed using a Transwell invasion assay. (E) Apoptotic rates analyzed by Annexin V-FITC/PI flow cytometry. (F) Levels of TNF-α, IL-6, and IL-1β quantified by ELISA. Data are presented as mean $\pm$ SD. *$p < 0.05$, **$p < 0.01$, ***$p < 0.001$. MTT, 3-(4,5-dimethylthiazol-2-yl)-2,5-diphenyltetrazolium bromide.

< 0.05). RT-qPCR confirmed robust increases in *BBOX* mRNA levels following lentiviral overexpression (Fig. 6B; $p < 0.05$), confirming successful overexpression. Restoration of BBOX attenuated mitochondrial oxidative stress, evidenced by reduced ROS levels detected using the green fluorescent probe BBcellProbe® OM09. (Fig. 6C; $p <$ 0.05). JC-1 staining further demonstrated that BBOX overexpression improved mitochondrial membrane potential, reversing TMAVA-induced depolarization (Fig. 6D; $p <$ 0.05). Metabolic function was partially restored, as indicated by elevated intracellular ATP and carnitine levels in the *BBOX* group compared with TMAVA alone (Fig. 6E; $p < 0.05$). Similarly, the NADPH/NADP$^+$ ratio, decreased by TMAVA, was significantly improved by BBOX restoration (Fig. 6F; $p < 0.05$), indicating improved redox balance. Western blot analysis further revealed that

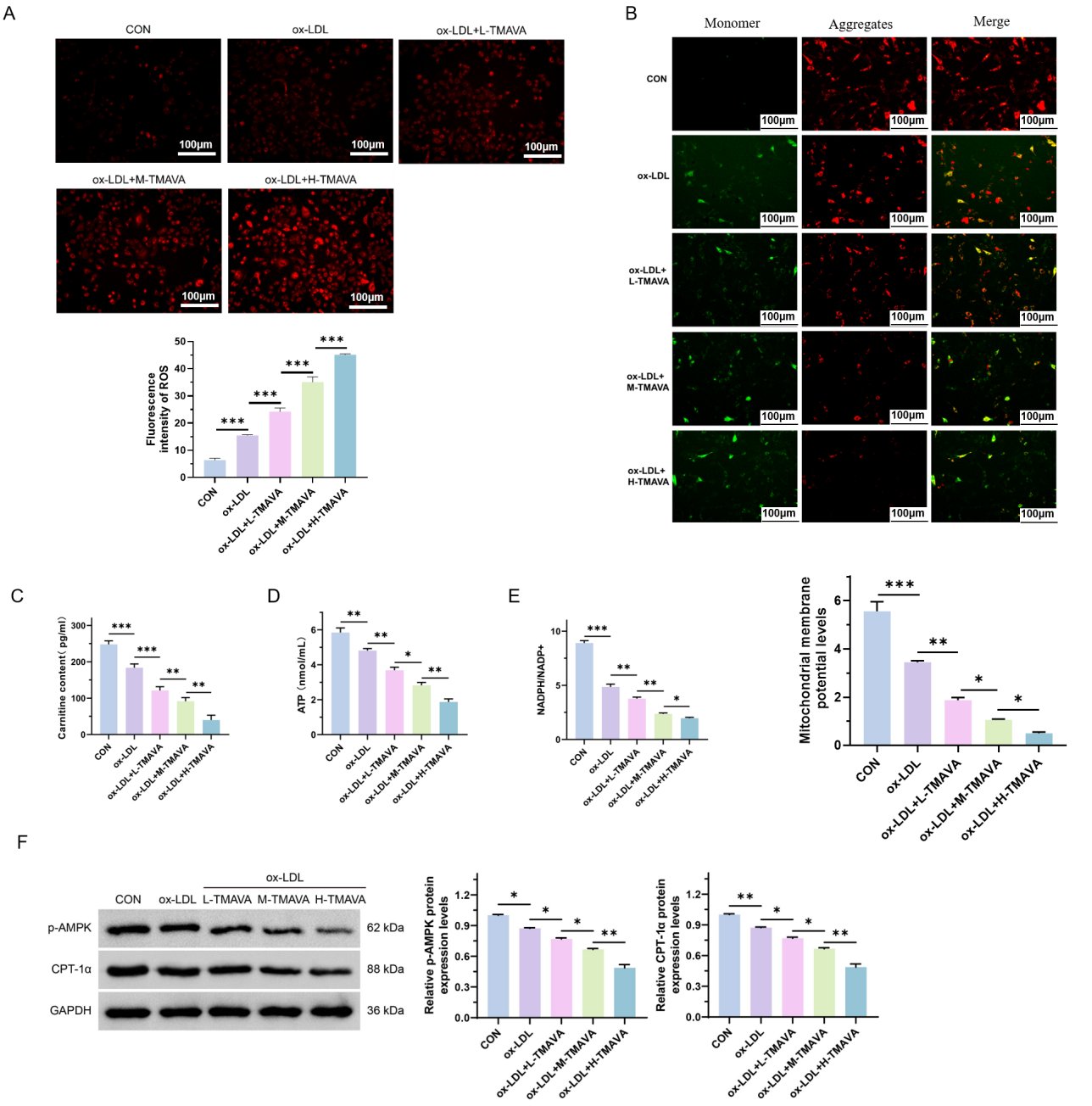

Fig. 5. TMAVA aggravates mitochondrial dysfunction and suppresses fatty acid oxidation in ox-LDL-treated HUVECs. (A) Representative fluorescence images and quantification of mitochondrial ROS levels assessed using Mito-Tracker Red CMXRos staining. (B) Representative JC-1 staining images (monomer, aggregate, and merged) and quantification of mitochondrial membrane potential ($\Delta\Psi$m). (C) Intracellular carnitine levels measured by ELISA. (D) Intracellular ATP levels measured by ELISA. (E) NADPH/NADP$^+$ ratio assessed by WST-8 assay and mitochondrial membrane potential quantified from JC-1 fluorescence ratio. (F) Western blot analysis of p-AMPK and CPT1α protein expression with GAPDH as the loading control, and densitometric quantification of relative protein expression. Data are presented as mean $\pm$ SD. *$p < 0.05$, **$p < 0.01$, ***$p < 0.001$.

BBOX overexpression reversed TMAVA-induced suppression of p-AMPK and CPT1α, restoring mitochondrial energy metabolism and fatty acid oxidation (Fig. 6G; $p < 0.05$).

Collectively, these findings indicate that *BBOX* overexpression alleviates TMAVA-induced mitochondrial dysfunction by restoring carnitine metabolism, redox homeostasis, and energy pathway activity.

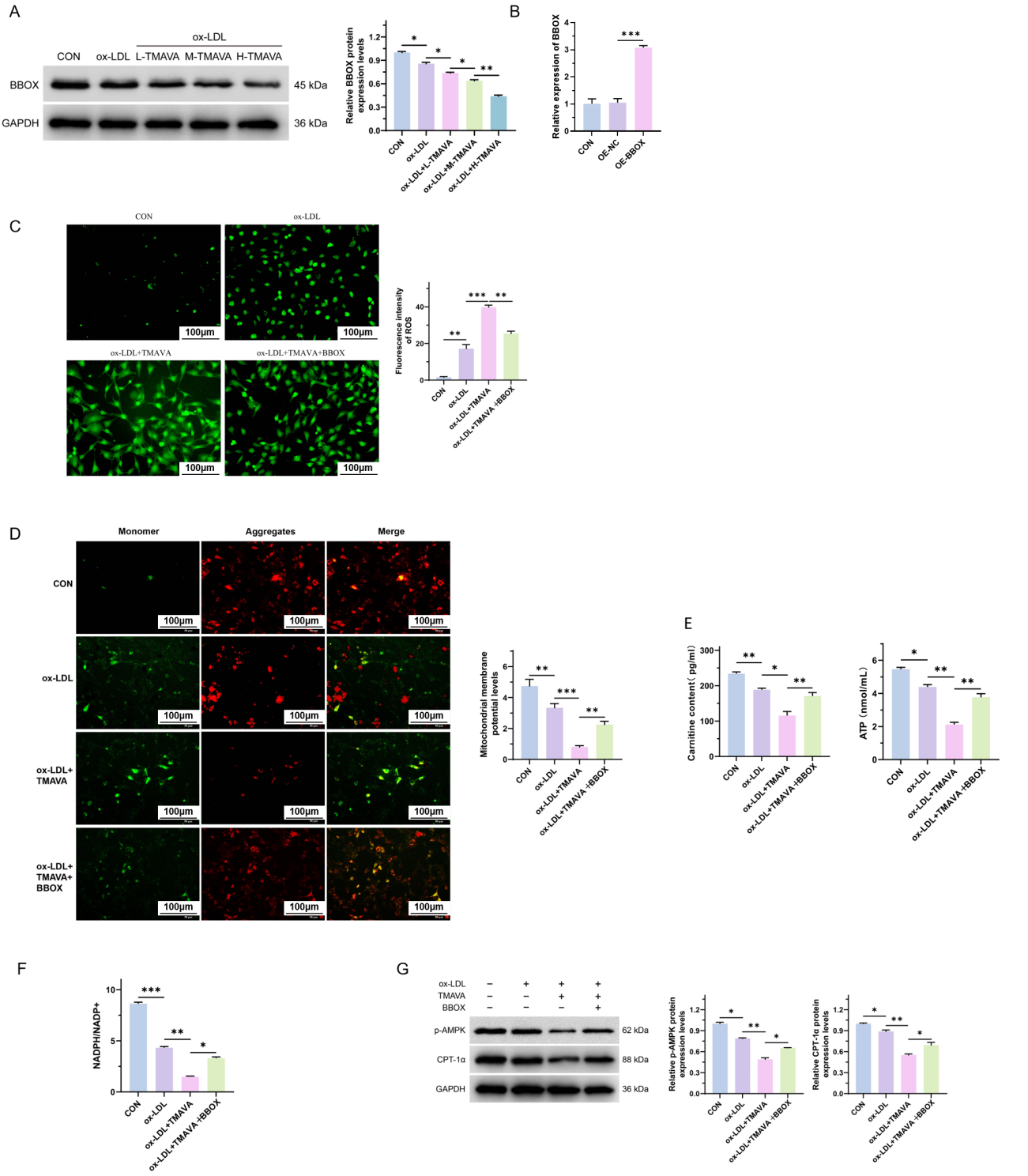

Fig. 6. BBOX overexpression restores carnitine metabolism and mitochondrial function in TMAVA-treated HUVECs. (A) Western blot analysis of BBOX protein expression after TMAVA treatment under ox-LDL stimulation. (B) RT-qPCR validation of BBOX mRNA overexpression following lentiviral transduction. (C) Representative fluorescence images and quantification of mitochondrial ROS levels. (D) Representative JC-1 staining images (monomer, aggregates, and merged) and quantification of mitochondrial membrane potential ($\Delta\Psi m$). (E) Intracellular carnitine and ATP concentrations measured by ELISA. (F) NADPH/$NADP^+$ ratio determined using a colorimetric WST-8 assay. (G) Western blot and densitometric quantification of p-AMPK and CPT1α protein expression, with GAPDH as the loading control. Data are presented as mean $\pm$ SD. *$p < 0.05$, **$p < 0.01$, ***$p < 0.001$.

BBOX Overexpression Ameliorates TMAVA-Induced Dyslipidemia and Vascular Inflammation in ApoE$^{-/-}$ Mice

To determine the effect of BBOX on TMAVA-induced metabolic and inflammatory disturbances *in vivo*, *BBOX* mRNA expression was first assessed in aortic tissues. As shown in Fig. 7A, *BBOX* mRNA was significantly reduced in the HFD group compared with controls ($p < 0.05$), further decreased by TMAVA ($p < 0.05$), and restored upon *BBOX* overexpression ($p < 0.05$). Serum lipid profiles (Fig. 7B) demonstrated that HFD markedly increased TC, TG, and LDL-C while reducing HDL-C ($p < 0.05$). These changes were further exacerbated by TMAVA ($p < 0.05$), whereas *BBOX* overexpression partially reversed the abnormalities ($p < 0.05$), indicating metabolic rescue. To assess vascular inflammation, mRNA levels of *IL-6*, *TNF-*α, and *IL-1*β were significantly elevated in HFD mice ($p < 0.05$), further enhanced by TMAVA ($p < 0.05$), and effectively suppressed by *BBOX* overexpression (Fig. 7C; $p < 0.05$). At the protein level (Fig. 7D), Western blot analysis confirmed these results, showing cytokine expression attenuated in the *BBOX* group despite TMAVA exposure.

Collectively, these findings demonstrate that *BBOX* overexpression alleviates TMAVA-induced dyslipidemia and vascular inflammation in ApoE$^{-/-}$ mice.

Discussion

This study demonstrated that the gut microbiota-derived metabolite TMAVA exacerbates endothelial dysfunction and vascular injury by disrupting mitochondrial metabolism in atherosclerosis. Using a high-fat diet-induced ApoE$^{-/-}$ mouse model and ox-LDL-stimulated HUVECs, we observed that TMAVA aggravated lipid dysregulation, mitochondrial dysfunction, oxidative stress, and inflammatory activation. Mechanistically, TMAVA significantly downregulated the expression of BBOX, a key enzyme in carnitine biosynthesis, in both aortic tissue and vascular endothelial cells. This suppression reduced intracellular carnitine levels, impaired fatty acid oxidation, decreased ATP production, and increased NADP$^+$/NADPH ratio. Key metabolic regulators, including p-AMPK and CPT1α, were also downregulated, reflecting compromised mitochondrial energy homeostasis. These alterations were accompanied by elevated mitochondrial ROS, membrane depolarization, enhanced apoptosis, and upregulation of pro-inflammatory cytokines. Notably, BBOX overexpression reversed most TMAVA-induced abnormalities, restoring mitochondrial function and attenuating inflammation. Taken together, these findings highlight the TMAVA-BBOX-carnitine axis as a crucial pathway linking microbial metabolites to vascular injury.

Our mechanistic findings support the hypothesis that TMAVA disrupts mitochondrial fatty acid oxidation primarily via BBOX inhibition. TMAVA has previously been identified as an endogenous inhibitor of BBOX, impairing fatty acid metabolism in hepatic tissues [20]. Consistent with these findings, we observed marked suppression of BBOX expression by TMAVA at both transcript and protein levels, validating it as a downstream effector. As expected, carnitine levels declined in TMAVA-treated cells, consistent with impaired β-oxidation. Carnitine is essential for transporting long-chain fatty acids into mitochondria for β-oxidation, and its deficiency has been strongly linked to impaired energy metabolism in cardiovascular tissues [21]. In the present study, ATP depletion and an increased NADP$^+$/NADPH ratio indicated a shift toward oxidative stress and energy failure. Furthermore, suppression of p-AMPK and CPT1α expression supports the proposal that TMAVA disrupts central regulators of mitochondrial metabolism. These results align with previous reports implicating AMPK-CPT1α signaling in endothelial energy homeostasis and inflammation control [22].

Mitochondrial dysfunction also manifested as elevated ROS levels and loss of membrane potential in our ox-LDL-stimulated HUVEC model treated with TMAVA. These findings are consistent with previous reports indicating that mitochondrial oxidative stress is a major driver of endothelial injury [23,24]. Moreover, our study demonstrated that these mitochondrial defects were accompanied by increased apoptosis and enhanced expression of pro-inflammatory factors, including IL-6, TNF-α, and IL-1β, at the transcript and protein levels. These inflammatory mediators contribute to atherosclerosis development and progression and are activated through ROS-dependent pathways. Restoration of BBOX expression effectively reversed mitochondrial dysfunction, reduced ROS accumulation, and suppressed cytokine production, thereby confirming that TMAVA promotes vascular inflammation via a BBOX-dependent mechanism. Together, these findings and previous evidence support a sequential mechanism: elevated TMAVA suppresses BBOX, reduces carnitine availability, impairs fatty acid oxidation, and disrupts mitochondrial function, ultimately exacerbating inflammation and vascular injury. This pathway provides a comprehensive explanation for the endothelial dysfunction and metabolic disturbances observed in our atherosclerosis model.

This study provides several novel insights into the metabolic regulation of vascular injury and atherosclerosis. First, it is the first to present experimental evidence linking microbiota-derived metabolite TMAVA to vascular mitochondrial dysfunction and inflammatory activation. Although TMAVA has previously been associated with hepatic lipid metabolism, its direct impact on vascular endothelial cells and atherosclerotic progression had not been defined [13]. By integrating *in vivo* ApoE$^{-/-}$ mouse models with *in vitro* endothelial cell assays, we comprehensively demonstrate that TMAVA exerts a detrimental effect on vascular homeostasis. Second, our study reveals the pivotal role of BBOX in maintaining mitochondrial

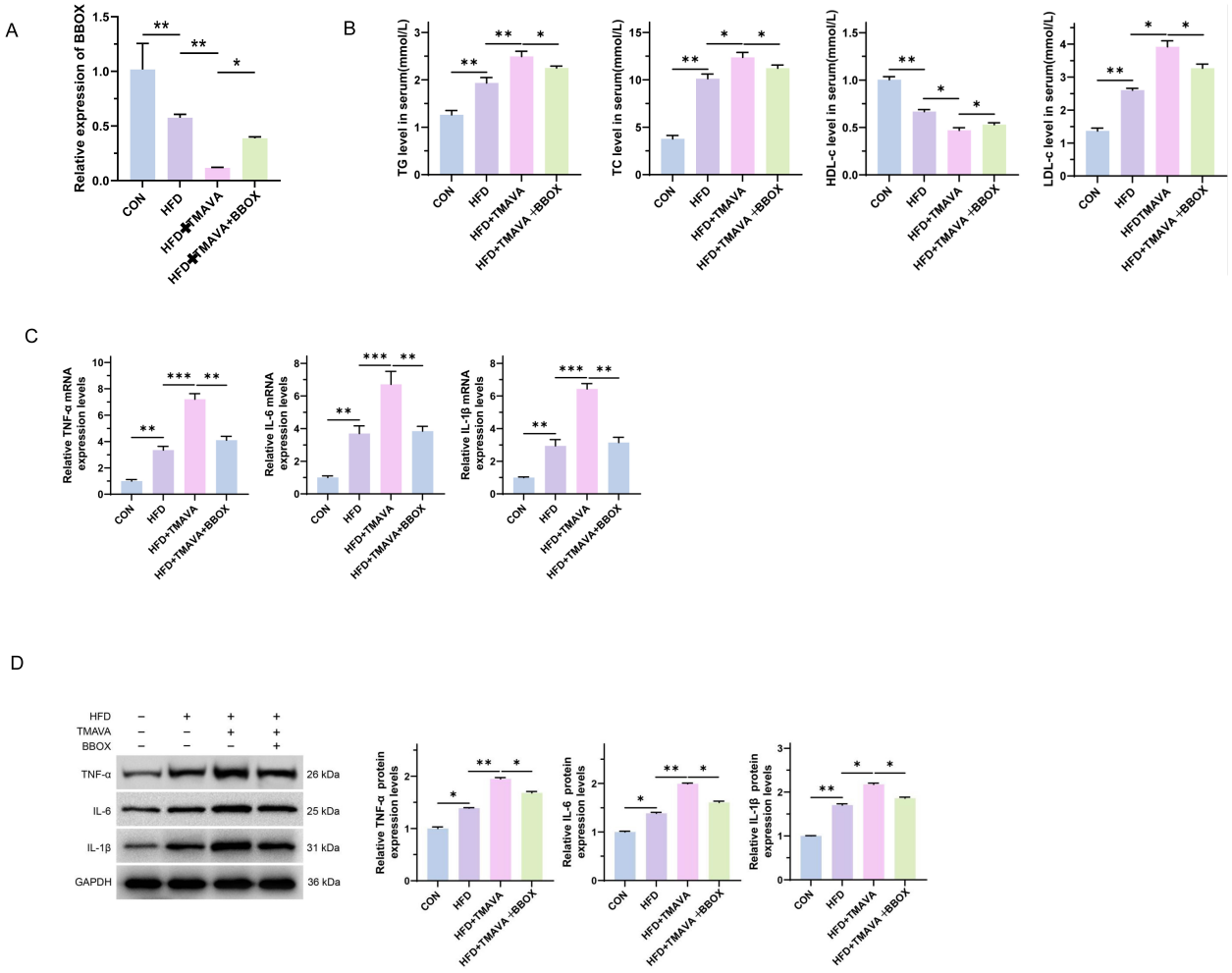

Fig. 7. *BBOX* overexpression mitigates TMAVA-induced dyslipidemia and vascular inflammation in ApoE$^{-/-}$ mice. (A) *BBOX* mRNA expression in aortic tissue determined by RT-qPCR. (B) Serum levels of TC, HDL-C, TG, and LDL-C measured by ELISA. (C,D) mRNA and protein expression levels of IL-6, TNF-α, and IL-1β in aortic tissue analyzed by RT-qPCR and Western blot analyses, with GAPDH as the loading control. Data are expressed as mean $\pm$ SD. *$p < 0.05$, **$p < 0.01$, ***$p < 0.001$.

fatty acid oxidation in endothelial cells. While the enzymatic role of BBOX in carnitine biosynthesis is well established, its significance in vascular energy regulation has received little attention. We demonstrate that BBOX suppression leads to reduced carnitine availability, impaired FAO, energy depletion, and oxidative stress in vascular cells. These findings position BBOX as a key node in the microbial metabolite-host mitochondrial axis [10,25]. Finally, we demonstrate that BBOX overexpression rescues TMAVA-induced dysfunction, offering a potential therapeutic strategy to mitigate gut metabolite-driven vascular injury. Collectively, these findings support a novel microbiota-metabolite-mitochondria regulatory axis in the pathogenesis of atherosclerosis.

Despite these insights, several limitations should be acknowledged. First, the translational relevance of TMAVA in human cardiovascular disease requires validation in clinical cohorts. Second, although TMAVA downregulates BBOX at both transcript and protein levels, the precise regulatory mechanism, whether transcriptional, post-transcriptional, or post-translational, remains unresolved. Third, our work focused on endothelial cells, given their central role as early responders to circulating microbial metabolites. However, atherosclerosis also involves macrophages and vascular smooth muscle cells, and future studies should extend to these populations. Additionally, although lipid metabolism, inflammation, and mitochondrial function were comprehensively assessed in ApoE$^{-/-}$ mice, we did not perform gross or histological analyses of aortic plaques. Nevertheless, the molecular and functional data strongly support the pathogenic role of TMAVA. Finally, pharmacologic approaches to enhance BBOX activity or restore carnitine metabolism may represent promising therapeutic interventions.

Conclusion

In summary, this study identifies TMAVA as a critical microbial metabolite that accelerates atherosclerosis by suppressing BBOX, thereby impairing carnitine biosynthesis and mitochondrial fatty acid oxidation. This disruption results in compromised energy production, oxidative stress, and vascular inflammation. Our findings highlight the TMAVA-BBOX-mitochondrial axis as a central mediator of endothelial dysfunction and suggest it as a potential therapeutic target. Future investigations should explore upstream regulatory pathways, diverse vascular cell types, and translational strategies for BBOX modulation.

Availability of Data and Materials

The datasets generated and analyzed during the current study are available from the corresponding author on reasonable request.

Author Contributions

ZM, DW and BN conceived and designed the study. ZM performed the experiments, analyzed the data, and drafted the manuscript. DW supervised the study and contributed to data interpretation and manuscript revision. WGL and YJG jointly contributed to the data acquisition and laboratory analysis of the work. All authors provided critical revisions for important intellectual content and approved the final version of the manuscript. All authors agreed to be accountable for all aspects of the work.

Ethics Approval and Consent to Participate

In compliance with NIH Guidelines, all animal protocols were approved by the Institutional Animal Care and Use Committee of the Guangdong Provincial Center for Laboratory Animals (No. D202506-13).

Acknowledgment

Not applicable.

Funding

This research was supported by 2024 Fuyang Health Research Project (No.FYHR2024-007).

Conflict of Interest

The authors declare no conflict of interest.

Supplementary Material

Supplementary material associated with this article can be found, in the online version, at https://doi.org/10.24976/Discov.Med.202537202.224.

References

[1] GBD 2019 Risk Factors Collaborators. Global burden of 87 risk factors in 204 countries and territories, 1990-2019: a systematic analysis for the Global Burden of Disease Study 2019. Lancet. 2020; 396: 1223–1249. https://doi.org/10.1016/S0140-6736(20)30752-2.

[2] Vaduganathan M, Mensah GA, Turco JV, Fuster V, Roth GA. The Global Burden of Cardiovascular Diseases and Risk: A Compass for Future Health. Journal of the American College of Cardiology. 2022; 80: 2361–2371. https://doi.org/10.1016/j.jacc.2022.11.005.

[3] Center For Cardiovascular Diseases The Writing Committee Of The Report On Cardiovascular Health And Diseases In China N. Report on Cardiovascular Health and Diseases in China 2023: An Updated Summary. Biomedical and Environmental Sciences. 2024; 37: 949–992. https://doi.org/10.3967/bes2024.162.

[4] Zhou M, Wang H, Zeng X, Yin P, Zhu J, Chen W, *et al*. Mortality, morbidity, and risk factors in China and its provinces, 1990-2017: a systematic analysis for the Global Burden of Disease Study 2017. Lancet. 2019; 394: 1145–1158. https://doi.org/10.1016/S0140-6736(19)30427-1.

[5] Nevoit G, Jarusevicius G, Potyazhenko M, Mintser O, Bumblyte IA, Vainoras A. Mitochondrial Dysfunction and Atherosclerosis: The Problem and the Search for Its Solution. Biomedicines. 2025; 13: 963. https://doi.org/10.3390/biomedicines13040963.

[6] Liu Z, Huang N, Liu C, Wu C, Zhou L, Liu X, *et al*. Mitochondrial DNA in atherosclerosis research progress: a mini review. Frontiers in Immunology. 2025; 16: 1526390. https://doi.org/10.3389/fimmu.2025.1526390.

[7] Murphy MP, Hartley RC. Mitochondria as a therapeutic target for common pathologies. Nature Reviews. Drug Discovery. 2018; 17: 865–886. https://doi.org/10.1038/nrd.2018.174.

[8] Tatmatsu-Rocha JC, Mendes-Costa LS. Inflammatory markers, oxidative stress, and mitochondrial dynamics: Repercussions on coronary artery disease in diabetes. World Journal of Diabetes. 2024; 15: 1853–1857. https://doi.org/10.4239/wjd.v15.i9.1853.

[9] Yan H, Hu Y, Lyu Y, Akk A, Hirbe AC, Wickline SA, *et al*. Augmented expression of superoxide dismutase 2 mitigates progression and rupture of experimental abdominal aortic aneurysm. Theranostics. 2025; 15: 4016–4032. https://doi.org/10.7150/thno.104957.

[10] Wang Z, Zhao Y. Gut microbiota derived metabolites in cardiovascular health and disease. Protein & Cell. 2018; 9: 416–431. https://doi.org/10.1007/s13238-018-0549-0.

[11] Liu Y, Xu L, Yang Z, Wang D, Li T, Yang F, *et al*. Gut-muscle axis and sepsis-induced myopathy: The potential role of gut microbiota. Biomedicine & Pharmacotherapy. 2023; 163: 114837. https://doi.org/10.1016/j.biopha.2023.114837.

[12] Wei J, Luo J, Yang F, Dai W, Huang Z, Yan Y, *et al*. Comparative genomic and metabolomic analysis reveals the potential of a newly isolated Enterococcus faecium B6 involved in lipogenic effects. Gene. 2024; 927: 148668. https://doi.org/10.1016/j.gene.2024.148668.

[13] Zhao M, Zhao L, Xiong X, He Y, Huang W, Liu Z, *et al*. TMAVA, a Metabolite of Intestinal Microbes, Is Increased in Plasma From Patients With Liver Steatosis, Inhibits γ-Butyrobetaine Hydroxylase, and Exacerbates Fatty Liver in Mice. Gastroenterology. 2020; 158: 2266–2281.e27. https://doi.org/10.1053/j.gastro.2020.02.033.

[14] Zhao Y, Lv H, Yu C, Liang J, Yu H, Du Z, *et al*. Systemic inhibition of mitochondrial fatty acid β-oxidation impedes zebrafish ventricle regeneration. Biochimica et Biophysica Acta. Molecular Basis of Disease. 2024; 1870: 167442. https://doi.org/10.1016/j.bbadis.2024.167442.

[15] Gander J, Carrard J, Gallart-Ayala H, Borreggine R, Teav T,

Infanger D, *et al*. Metabolic Impairment in Coronary Artery Disease: Elevated Serum Acylcarnitines Under the Spotlights. Frontiers in Cardiovascular Medicine. 2021; 8: 792350. https://doi.org/10.3389/fcvm.2021.792350.

[16] Zhao M, Wei H, Li C, Zhan R, Liu C, Gao J, *et al*. Gut microbiota production of trimethyl-5-aminovaleric acid reduces fatty acid oxidation and accelerates cardiac hypertrophy. Nature Communications. 2022; 13: 1757. https://doi.org/10.1038/s41467-022-29060-7.

[17] Yan R, Zhang X, Xu W, Li J, Sun Y, Cui S, *et al*. ROS-Induced Endothelial Dysfunction in the Pathogenesis of Atherosclerosis. Aging and Disease. 2024; 16: 250–268. https://doi.org/10.14336/AD.2024.0309. (online ahead of print)

[18] Geng S, Lu R, Zhang Y, Wu Y, Xie L, Caldwell BA, *et al*. Monocytes Reprogrammed by 4-PBA Potently Contribute to the Resolution of Inflammation and Atherosclerosis. Circulation Research. 2024; 135: 856–872. https://doi.org/10.1161/CIRCRESAHA.124.325023.

[19] Fan X, Li Q, Wang Y, Zhang DM, Zhou J, Chen Q, *et al*. Non-canonical NF-κB contributes to endothelial pyroptosis and atherogenesis dependent on IRF-1. Translational Research. 2023; 255: 1–13. https://doi.org/10.1016/j.trsl.2022.11.001.

[20] Zhang Q, Xing W, Wang Q, Tang Z, Wang Y, Gao W. Gut microbiota-mitochondrial inter-talk in non-alcoholic fatty liver disease. Frontiers in Nutrition. 2022; 9: 934113. https://doi.org/10.3389/fnut.2022.934113.

[21] Robert A, Moury J, Nendumba G, Hauqiert B, Vornicu O, Blackman S, *et al*. Carnitine deficiency in intensive care unit patients undergoing continuous renal replacement therapy-An underrecognized issue with potential for severe complications. Journal of Intensive Medicine. 2025; 5: 249–251. https://doi.org/10.1016/j.jointm.2024.12.002.

[22] Neumann D, Viollet B. AMP-Activated Protein Kinase Signalling. International Journal of Molecular Sciences. 2019; 20: 766. https://doi.org/10.3390/ijms20030766.

[23] Xie T, Wang C, Jin Y, Meng Q, Liu Q, Wu J, *et al*. CoenzymeQ10-Induced Activation of AMPK-YAP-OPA1 Pathway Alleviates Atherosclerosis by Improving Mitochondrial Function, Inhibiting Oxidative Stress and Promoting Energy Metabolism. Frontiers in Pharmacology. 2020; 11: 1034. https://doi.org/10.3389/fphar.2020.01034.

[24] Mohamud Yusuf A, Borbor M, Hussner T, Weghs C, Kaltwasser B, Pillath-Eilers M, *et al*. Acid sphingomyelinase inhibition induces cerebral angiogenesis post-ischemia/reperfusion in an oxidative stress-dependent way and promotes endothelial survival by regulating mitochondrial metabolism. Cell Death & Disease. 2024; 15: 650. https://doi.org/10.1038/s41419-024-06935-9.

[25] Longo N, Frigeni M, Pasquali M. Carnitine transport and fatty acid oxidation. Biochimica et Biophysica Acta. 2016; 1863: 2422–2435. https://doi.org/10.1016/j.bbamcr.2016.01.023.